Invited Paper

Doped silicon-based broadband terahertz absorber: a review

XiaoFei Zang, YiMing Zhu *, and Songlin Zhuang
Shanghai Key Lab of Modern Optical System, Engineering Research Center of Optical Instrument and System, Ministry of Education, University of Shanghai for Science and Technology, 516, Jungong Rd. Yangpu Dist. Shanghai, China, 200093
* Email: ymzhu@usst.edu.cn

(Received August 18, 2015)

Abstract: Wideband absorption with high efficiency has attracted much attention due to the potential applications in imaging, anti-radar cloaking devices, sensors, detectors, and so on. Recently, meta-based periodical resonance structure (metamaterials) is proposed to realize perfect absorber. However, it suffers from the absorption of terahertz (THz) waves just in the single-frequency or narrow band width owing to its resonance features. Here, in this review, we discuss various THz broadband absorbers by fabricating gratings on heavily boron-doped silicon substrate. By optimizing the grating structure, the absorption bandwidths are 1 *THz*, 1.5 *THz*, and 2.0 *THz*, respectively with absorbance above 95%.

Keywords: Terahertz absorber, First-order diffraction, Second-order diffraction, Air-gap mode.

doi: 10.11906/TST.129-144.2015.12.13

1. Introduction

In the past few years, one of the most hot-topics of perfect absorber has attracted much attention. As a useful functional device, it can be applied into imaging, sensors, detectors, modulator, anti-radar cloaking devices, etc [1-8]. A perfect absorber means that all incident radiation is almost absorbed at the operating frequency. And, the first perfect absorber is proposed by N. I. Landy in 2008 [9]. It is a typical sandwich structure which is composed of a split electric resonant ring (ERR) and a metal-strip substrate separated with a loss dielectric spacer. The ERR and the metal-strip can individually absorb the electric and magnetic components of an incident electromagnetic wave. By optimizing the structure of the SRR and the metal-strip, the unit cell can achieve zero reflection because it can have an impedance equal to the free space value $Z=\sqrt{\mu/\varepsilon}=1$. The fundamental principle of this micro-wave perfect absorber is similar to the perfectly matched layer absorbing boundary condition, which splits wave incident upon a boundary into electric and magnetic components to obtain a near unity absorber. And, such a structure is quickly extended to THz regime by using slight smaller dimensions to achieve THz absorber [10-11]. The physical mechanism of such THz perfect absorber is quite the same as the above microwave perfect absorber: the incident electric field and magnetic field are strongly coupled to the ERR and split wire, leading to antiparallel currents in the split wire and ERR. Meanwhile, based on perfectly impedance matched negative index material and the resonance wires, the near-infrared (NIR) absorber consisting of a cut wire surrounded by two continuous wires was proposed [12]. Different from the above polarization-dependent perfect absorbers, polarization-independent perfect absorbers are proposed in micro-wave, THz, NIR and optical wavelengths [13-26]. Furthermore, the multi-band such as dual- band and triple-band absorbers are also investigated [27-30].

In addition to the above single-frequency and multi-frequency absorbers, ultra-compact, polarization-independent and wideband absorbers are now pursuit goals of many researchers [31-34]. For example, Huang *et al*., reported a wideband THz absorber which consists of two sets of structures resonating at different but close frequencies [31]. So, the overall absorption spectrum is the superposition of individual components and becomes flat at the top over a significant bandwidth. Wu *et al.*, proposed a broadband absorber by introducing three subunits with various sizes in a unit cell, resulting in nearly 100% absorbance at multiple adjacent frequencies and high absorbance over a broad frequency range [32]. Multiplexed plasmonic metal-based and dispersion engineering-based broadband absorbers are demonstrated in Ref [33, 34]. And, multi-layered and no- coplane meta-based ultra-broadband are also studied [35-38]. Recently, as a practical solution, R. Kakimi *et. al*., proposed a photonic-crystal slab, which can be easily fabricated with doped silicon, to capture of THz waves [39]. The incident THz waves can be coupled into the photonic-crystal slab because of the guided resonance (in-plane resonant modes). In addition, a mirror was introduced underneath the photonic-crystal slab to induce Fabry–Pérot resonance. By optimizing the lattice parameters, the guided resonance and the Fabry–Pérot resonance can be combined with each other, leading to a 50 *GHz* broadband THz absorber. Pu *et al*., theoretically designed another simple structure *i.e.*, doped silicon with square-shaped grating array, to realize a much wider bandwidth of THz absorption by virtue of the anti-reflection effects and the first-order diffraction [40]. And, Ma *et al*., demonstrated such a broadband THz absorber by fabricating square gratings on heavily boron-doped silicon substrate [41]. Here, in this paper, we review various THz broadband absorbers based on the heavily boron-doped silicon [42-44] .

2. Broadband THz absorber based on [±1, 0]-order diffraction

In this section, we discuss the broadband THz absorber based on the anti-reflection effects and the [±1, 0]-order diffraction. The realized absorber is designed by fabricating periodical square gratings on the heavily boron-doped silicon, as shown in Figs. 1(a) and 1(b). According to the Drude model, the complex permittivity of the Boron heavily-doped silicon can be represented as follows:

$$\varepsilon = \varepsilon_\infty + \frac{\omega_p^2}{\omega\left(\omega + \dfrac{j}{\tau}\right)}, \tag{1}$$

where j is the imaginary unit, ε_∞ =11.7 is the permittivity of the non-doped silicon, τ is the carrier relaxation time, and ω_p is the plasma frequency. For a 0.54 Ω cm Boron-doped silicon which we choose in our experiment, τ equals to 0.571 *ps* with ω_p=19.1 *THz*. The fundamental principal of such broadband THz absorber is shown in Fig. 1(c). In the low frequency regime, the incident THz waves cannot see the square grating clearly. So, in this case, the square doped-silicon grating can be considered as an effective medium coating on the substrate, and the absorption of THz waves is mainly attributed to the anti-reflection effect (destructive interference) between the incident and the reflected THz waves. In the high frequency regime, the grating should no longer be treated as a dielectric film, but instead as a periodic grating array, and in this situation, the [±1, 0]-order grating diffractions are contributed to the absorption of THz waves. By choosing the proper structure parameters, the anti-reflection effect and the [±1, 0]-order diffractions can be combined into each other, leading to a wide-bandwidth of THz absorber.

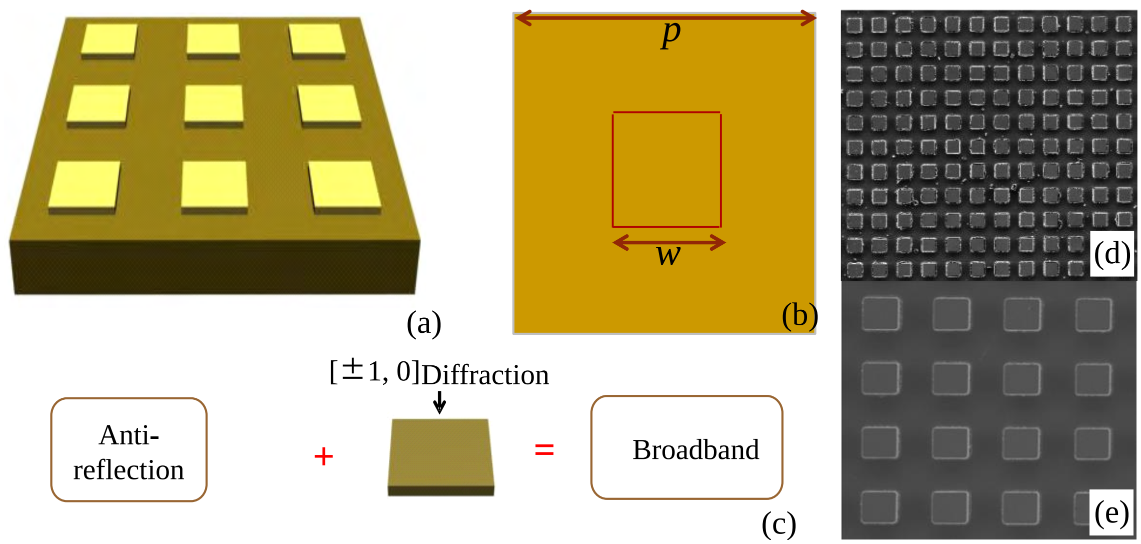

Fig. 1 Schematics illustrating the (a) periodical structure and (b) unit cell of the THz wave absorber. (c) The basic principal of THz wave absorption for broadband operation. (d) and (e) SEM of the fabricated periodical array slab.

We fabricate the THz absorber by utilizing the traditional photolithography and ICP etching process on a 0.54 Ω *cm* p-type silicon wafer, as shown in Figs. 1(d) and 1(e). A 1μm AZP4620 image reversal photoresist film was spin-coated and patterned using standard photolithography. Because there is an etch rate difference between the heavy-doped silicon and photoresist, the remained photoresist will perform as a mask to prevent the certain areas from etching. By etching for a proper time, the square grating structure is formed on the surface of the silicon. The structure parameters of the THz absorber are as follows: p=88 μm, w=45 μm and h=42 μm (the thickness of the grating).

Now, we investigate the transmission, reflection and the grating diffraction of our designed structure. Here, transfer matrix method [45] is used to demonstrate the high absorption characteristics of the substrate. Based on transfer matrix method, the transmittance and reflectance of a single layer will be calculated as:

$$R = \left| \frac{\frac{j\sin(kt)}{n} - jn\sin(kt)}{2\cos(kt) + \frac{j\sin(kt)}{n} + jn\sin(kt)} \right|^2, \quad T = \left| \frac{2}{2\cos(kt) + \frac{j\sin(kt)}{n} + jn\sin(kt)} \right|^2 \tag{2}$$

where t is the thickness of the bare substrate, $k=nk_0$ is the wave vector of THz wave in the dielectric layer with refractive index of n. the transmission and reflection spectrum for the substrate layer with different thickness are shown in Fig. 2(a) and 2(b). Obviously, over more

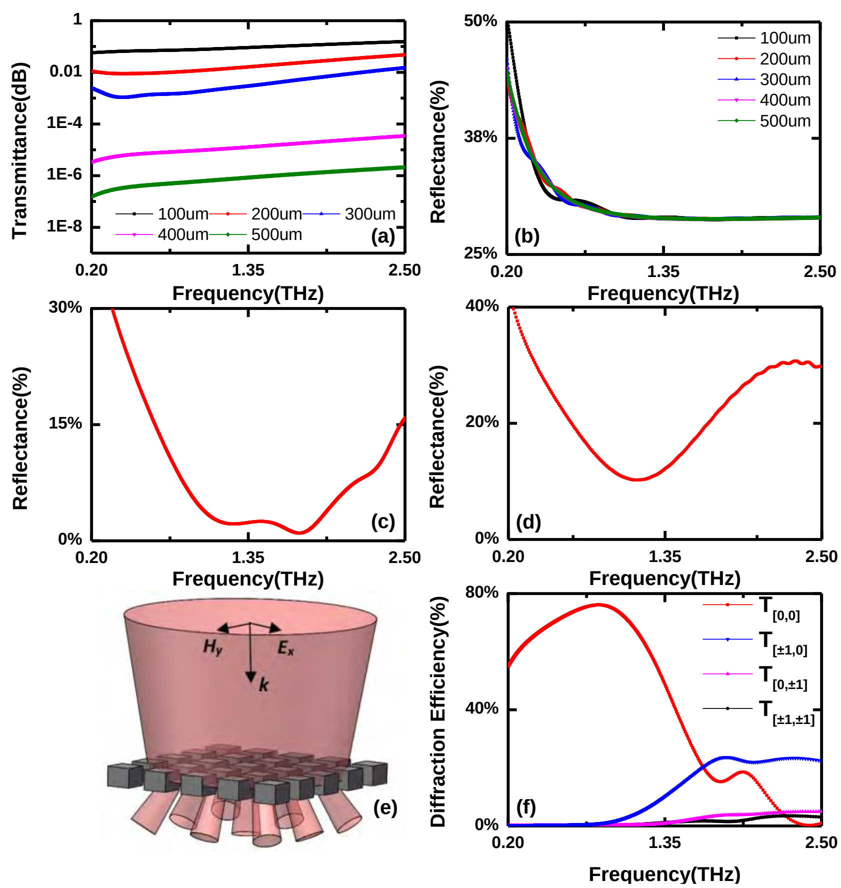

Fig. 2 The simulated results to illustrate how to control the transmission and reflection rate and frequency of the designed absorber: The transmission-spectrum (a) and the reflection- spectrum (b) of the substrate layer with different thickness. (c) The reflectance spectrum of the absorber. (d) The reflection spectrum of the absorber caused by the effective medium coating on the substrate. (e) The nine combinations of different diffraction orders for a 2D grating. (f) The diffraction efficiency of the absorber.

than 99% of the incident THz waves cannot propagate through the silicon substrate when the thickness exceeds 300 μm (Fig. 2(a)). However, the reflectance of the bare substrate is about 28% from 1 to 2.5 *THz*, and it is independent on the thickness of the substrate. So, we should design the periodic array on the substrate to further reduce the reflection (as shown in Fig. 1(a)). Here, two antireflection mechanisms are designed for the grating layer to decrease the reflection： the destructive interference(anti-reflection effects) and the [±1, 0]-order grating diffraction. The destructive interference happens on low frequency THz wave ($f<4p/c$) while the grating diffraction will affect the high frequency THz wave ($f>4p/c$) absorption. In the low THz regime, the grating layer is functioned as a thin dielectric layer since the wavelength of the low frequency THz wave is much larger than the scale of the grating structure. And, according to the effective medium theory (EMT) [46], the effective permittivity of a one-dimensional grating can be calculated as:

$$\varepsilon_{//} = (1-\mathrm{r})\varepsilon_{air} + r\varepsilon_{si}\,, \qquad \varepsilon_{\perp} = \frac{\varepsilon_{air}\varepsilon_{si}}{(1-r)\varepsilon_{si} + r\varepsilon_{air}}\,, \tag{3}$$

where $r=w/p$ is the filling factor of the grating structure. We can calculate the effective refraction index of the two-dimensional isotropic grating structure as introduced in Ref [47]. Hence, the structure of the absorber can be viewed as the heavily doped silicon substrate coating with a thin dielectric film which has a refractive index of n_{eff}. The reflection waves from the top and bottom surface of the thin film will cause the Fabry-Pérot interference at certain frequency. In this case, the destructive interference occurs at the frequency $f = c\times(2k+1) / (4n_{eff}d)$=1.17 *THz* ($k$ is integer), as shown in Fig. 2(d). This is matched with the left dip at f=1.17 *THz* shown in Fig. 2(c). So, in the low frequency regime, the high-absorption of the THz absorber can be attributed to the anti-reflection due to the destructive interference effects. In a high frequency region, effective medium theory no longer works. The grating should no longer be treated as a dielectric film, but instead as a periodic grating array. And, the grating of the absorber with the same parameters is analyzed by using the two dimensional rigorous coupled-wave analysis (2D-RCWA) method. Nine combinations of diffraction orders ([-1, -1], [-1, 0], [-1, 1]; [0, -1], [0, 0], [0, 1]; [1, -1], [1, 0], [1, 1]) are investigated (Fig. 2(e)). Fig. 2(f) illustrates the diffraction efficiency of different diffraction orders for the transverse magnetic (TM) polarization incident THz wave. The results (Fig. 2(e)) demonstrate that the [±1, 0]-order diffractions play a dominant role from 1.6 *THz*, and the maximum diffraction efficiency is at f=1.73 *THz*, which is matched with the right dip at f=1.73 *THz* shown in Fig. 2(c). The simulation results demonstrate that the effective medium plays a decisive role in the lower THz frequency while the grating diffraction behavior will gradually take more effect with the increasing of the frequency. Therefore, these two reflection dips (shown in Fig. 2(c)) will lead to two absorption peaks since the substrate can be regarded as a non-transmission layer.

The absorber is tested by the THz-TDS under both transmission-type mode (Fig. 3 (a)) and reflection-type mode (Fig. 3(b)). Such a THz-TDS system works from 0.2 *THz*-2.8 *THz* with a

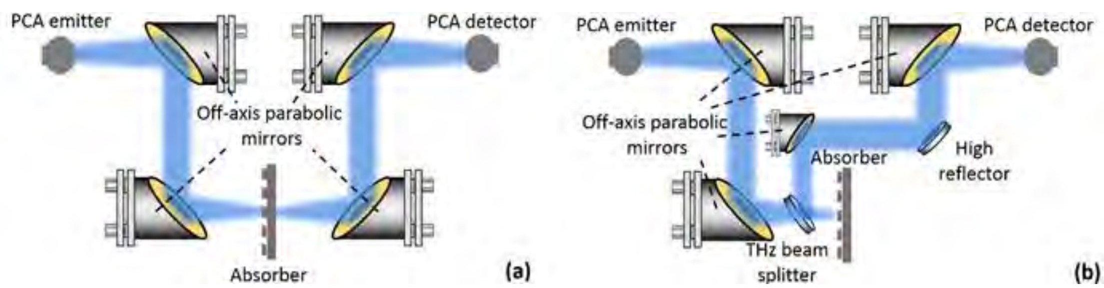

Fig. 3 The THz-TDS system used to test the transmittance and reflectance of the absorber: (a) the transmission-type mode, (b) the reflection-type mode.

4.75 *GHz* spectral resolution. The transmission-type system consists of two pairs of off-axis parabolic mirrors. The first two mirrors are able to focus the THz wave on the sample while the other two mirrors collect the wave which passes through the sample, and focuses on the detector. For the reflection-type system, a 50/50 *THz* beam splitter is added to collect the wave reflected from the sample. The behavior of the absorber is experimentally demonstrated by measuring the transmission and reflection of the sample. The transmission spectrum is shown in Fig. 4(a), while the reflection spectrum is shown in Fig. 4(b) (red lines). Both the measured results are good agreement with the simulation results (black lines) where the absorption efficiency can reach over 95% from 1 *THz* to 2 *THz*. In addition, the absorber is polarization-independent due to the two-dimensional symmetrical (Fig. 4(c)). Furthermore, the absorption spectrum of our terahertz absorber with different incident angles is also demonstrated, as shown in Fig. 4(d). The absorption is still greater than 90% for over a 1 *THz* bandwidth, when the incident angle is even close to 60^0.

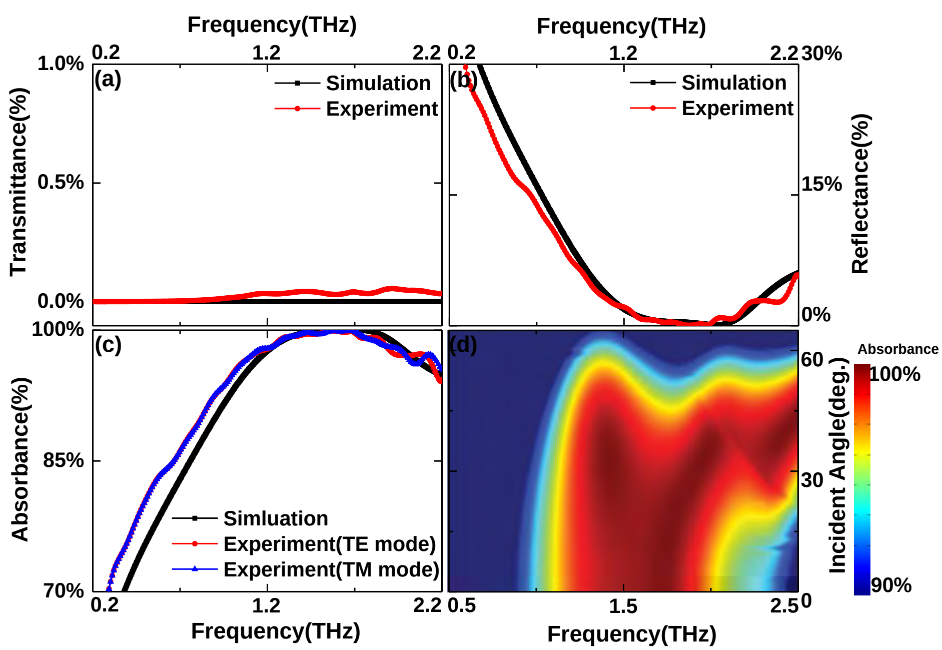

Fig. 4 The simulation and measurement results of the polarization-independent THz absorber: the transmission (a) the reflection (b) and the absorption (c) spectrum. (d)the absorption spectrum under different incident angle.

3. Broadband THz absorber based on orthogonal diffraction

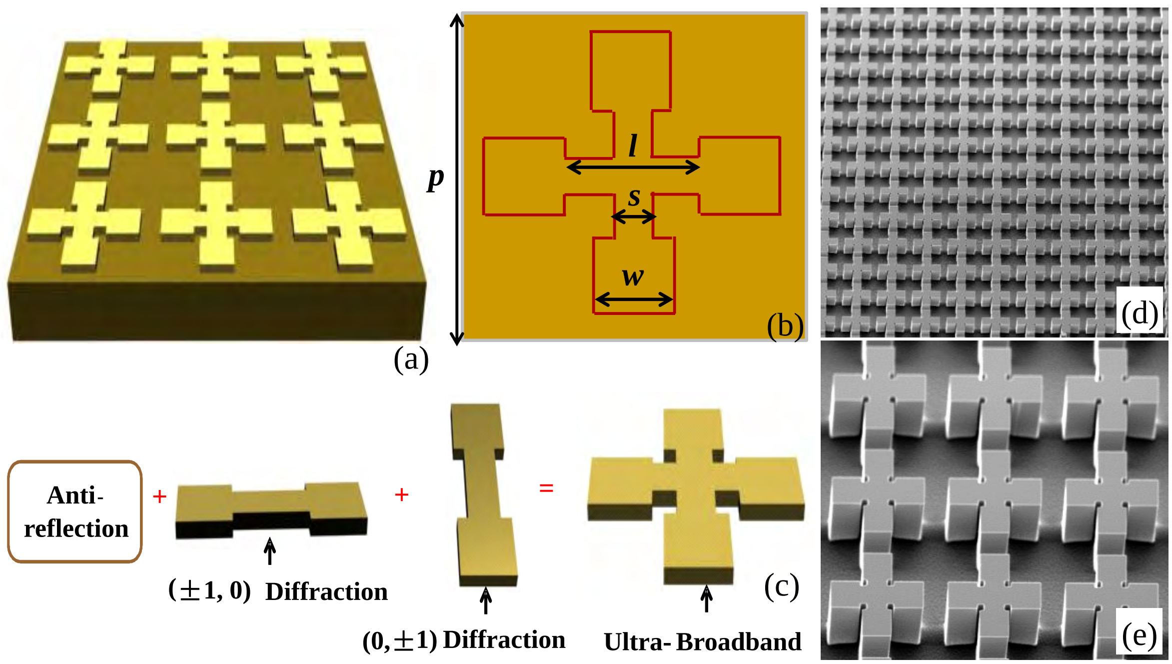

Fig.5 Schematics of the (a) periodical structure and (b) unit cell of the THz wave absorber. (c) The fundamental principal of the wideband THz wave absorber. (d) and (e) SEM of the fabricated periodical array slab.

In section 2, we study the broadband THz absorber by virtue of the anti-reflection effects and the [±1, 0]-order diffraction by fabricating square grating array on the substrate. However, the square-shaped grating array can just utilize the [±1, 0]-order grating diffraction, which suppresses the bandwidth of the absorber. In this section, the [±1, 0]-order and the [0, ±1]-order diffractions are all excited simultaneously to further enhance the absorption bandwidth. We design the two 90 degree crossed dumbbell-shaped doped-silicon grating arrays on the heavily-doped silicon-based substrate, as shown in Fig. 5(a) and 5(b). The basic principal of such broadband THz absorber is shown in Fig. 5(c). It is attributed to the anti-reflection effects (which is the same as the square grating in section 2), and especially the [±1, 0]-order and the [0, ±1]-order diffractions excited by the dumbbell-shaped doped-silicon grating arrays. In high frequency regime, the dumbbell-shaped strip arrays can be considered as two 90 degree crossed grating (the horizontal stripe and the vertical stripe grating array). So, the [±1, 0]-order and [0, ±1]-order grating diffractions are separately contributed to the absorption of THz waves. And, by optimizing the structure parameter, the resonance absorptions induced by the anti-reflection effects, the [±1, 0]-order, and the [0, ±1]-order diffractions can be jointed into a broadband absorption. Here, in this section, the optimized structure parameters are as follows: p=96 μm, l=27 μm, s=17 μm, and w=25 μm. The thickness (h) of each dumbbell-shaped strip (pattern) and substrate are 38 μm and 462±10 μm, respectively. Such a kind of broadband THz absorber is also fabricated by the traditional photolithography and ICP etching process on a 0.54 $\Omega{\cdot}cm$ p-type silicon wafer (see Figs. 5(d) and 1(e)).

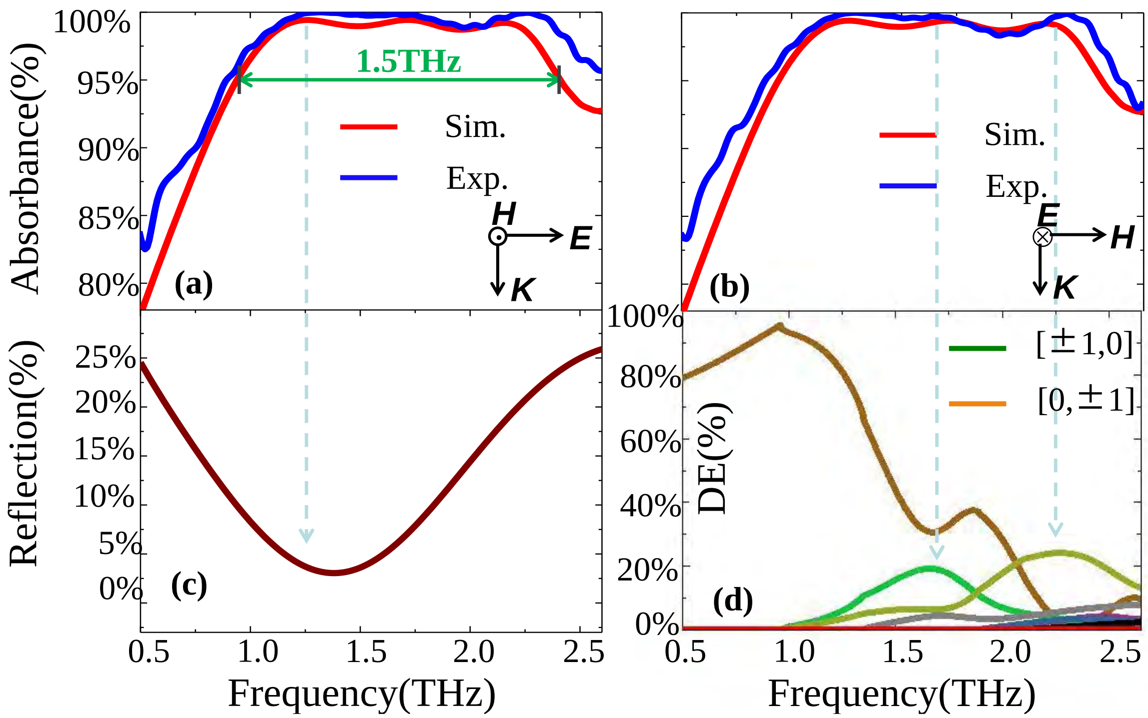

Fig. 6 The simulated (red line) and measured (blue line) results of the broadband THz absorber with (a) TE incident THz wave, and (b) TM incident THz wave. (c) The calculated reflection spectrum in the case of that the periodical array on top of the substrate is equivalent as an effective medium. (d) The diffraction efficiency (DE) of different diffraction orders. The inset in (a) is the quality factor of such periodical structure.

The calculated and measured absorption spectra for TE (transverse electric) and TM (transverse magnetic) incident THz wave are shown in Figs. 6(a) and 6(b), respectively. The measured results are also tested via the THz-TDS. For TE incident THz waves (see Fig. 6(a) of red line), the peak absorbance is about 99.3%, with the bandwidth~1.5 *THz* and absorbance ≥ 95%. The measured result in Fig. 6(a) (see the blue line) also appears over 1.5 *THz* bandwidth of trapping THz waves with absorbance ≥ 95%. And, both the calculated spectrum and the measured spectrum show good agreement, except for a slight difference in resonance frequency. Such discrepancy can be attributed to the structural difference between the fabricated sample, and the calculated model. When compared with Figs. 6(a) and 6(b), it is found that the absorption spectra are consistent with each other for both TE and TM normal incident THz waves. It means that the absorption of THz wave is insensitive to the polarization of the incident waves (for the normal incident), due to the symmetrical periodic structure. From Figs. 6(a) and 6(b), we can also find that there are three peaks in the absorption spectra at 1.265 *THz*, 1.72 *THz*, and 2.155 *THz*, respectively. Such a broad bandwidth trapping is closely combined with these three peaks. For f=1.265 *THz*, the wavelength of the incident THz wave is larger than the period of the structure, making the periodic array interpret as an effective medium, and, in this case, it can be considered as an effective medium coating on the substrate. So, we calculate the reflection spectrum of a doped-silicon substrate coating with such effective medium on its upper-surface, as shown in Fig. 6(c). It is a typical Fabry–Pérot shaped spectrum, and a dip nearly at f=1.265 *THz* with small reflection which is caused by the destructive interference between the reflected waves (In this situation, the incident THz wave is mainly absorbed in the grating array, and a little of the incident THz wave transmits into the substrate (see Figs. 7(a_1) and 7(a_2))). But, at high frequency regime, the reflection spectrum of Fig. 6(c) still shows a high reflection which is mismatched with the absorption characterizes in Figs. 6(a) and 6(b). So, the effective medium theory cannot be applied to the high frequency region. Based on 2D-RCWA method, we calculate the grating diffractions of the dumbbell-shaped grating, as shown in Fig. 6(d). The two peaks at f=1.72 *THz* and f=2.155 *THz* are mainly due to the [±1, 0]-order, [0, ±1]-order, and [0, 0]-order grating diffractions, respectively. The peak at f=1.72 *THz* is caused by the [±1, 0]-order grating diffraction through the smaller air gap between the horizontal doped-silicon strips (see Figs. 7(b_1) and 7(b_2)), and the [0, 0]-order grating diffraction through

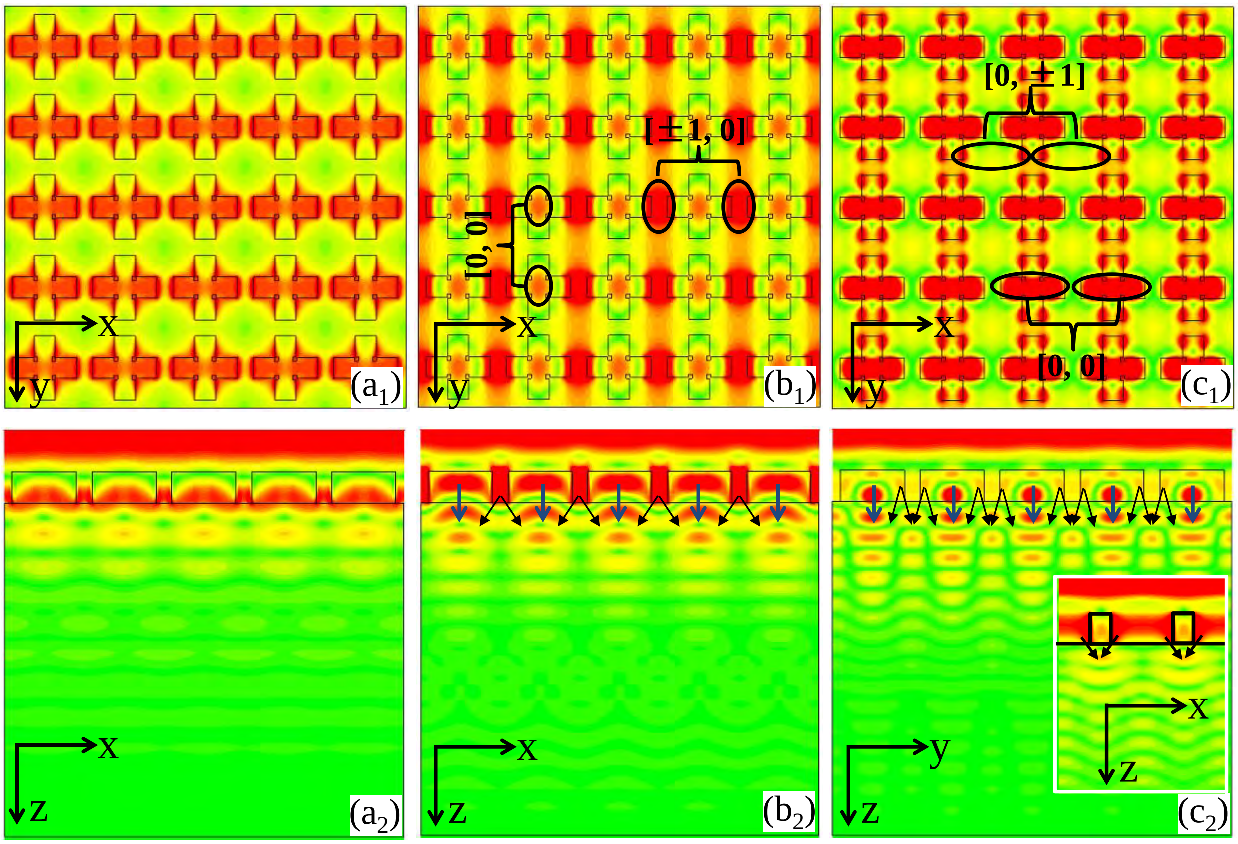

Fig. 7 The electric field distribution at the interface between the periodical arrays and the substrate for f=1.265 *THz* (a), f=1.688 *THz* (b) and f=2.135 *THz* (c), respectively. The inset in (c) is the electric field distribution at y=38 μm.

the vertical doped-silicon strips. The peak at f=2.155 *THz* is mainly caused by the [0, ±1]-order grating diffractions through the bigger horizontal air gap between the vertical dumbbell-shaped doped-silicon strips, and the [0, 0]-order grating diffraction through the horizontal dumbbell-shaped doped-silicon strips (see Figs. 7(c_1) and 7(c_2)). When we compare with Figs. 7(a_2), 7(b_2), and 7(c_2), significant field distributions transmit into the substrate (see Fig. 7(b_2) and 7(c_2)), which demonstrate that in the high-frequency regime, the periodical arrays can be considered as grating arrays and much of the incident waves is absorbed in substrate due to the grating diffraction.

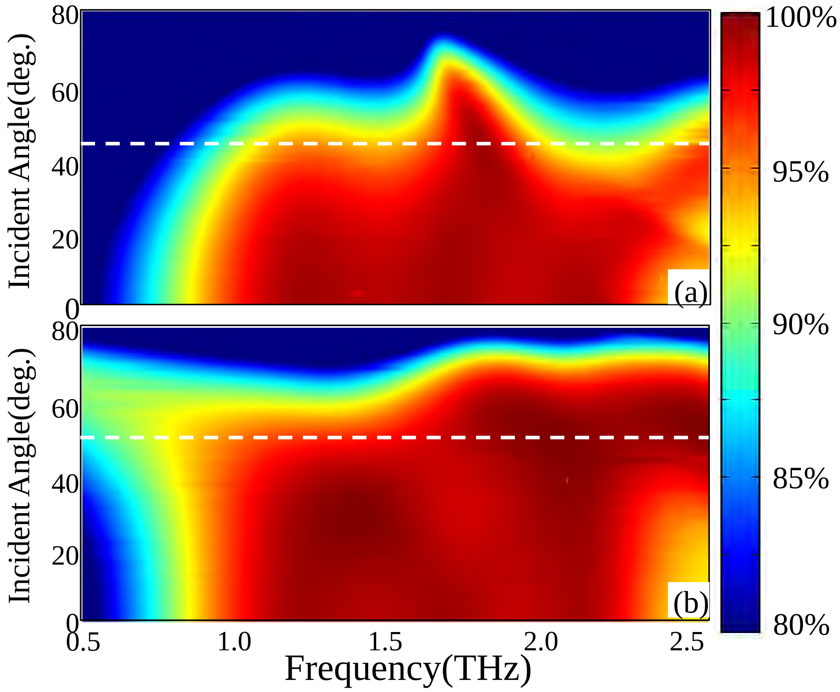

Fig.8 The absorption spectra under different incidence angles for (a)TE THz wave, and (b)TM THz wave.

In practical case, the incident THz wave isn't always incident normally to the THz absorber. Therefore, we should investigate the detailed absorption characterizes of this THz absorber at various incident angles, as shown in Fig. 8. For TE polarization, the maximum absorption is also above 90% with corresponding bandwidth of 1.5 *THz* even for incident angle as large as 45^0 (Fig. 8(a)). The absorption efficiency of TM polarization is over 95% with bandwidth of 1.5 *THz*, when the incident angle up to 45^0. All of these results illustrate that our designed THz absorber is insensitive to incident directions.

4. Ultra-broadband THz absorber by exciting high-order grating diffraction

In this section, we study the ultra-broadband THz absorber further by exciting the second-order grating diffraction. We propose a double-layered doped-silicon square grating array to realize such an ultra-broadband and polarization-independent THz absorber. Figures. 9(a) and 9(b) show the schematic of ultra-broadband THz absorber. It is a three-layered structure consisting of double-layered square grating array and substrate. And, we also use the traditional photolithography and ICP etching to fabricate the sample (see Figs. 9(c) and 9(d)). Figure 9(e) shows the fundament principle of the designed ultra-broadband THz absorber. Here, the ultra-broadband THz absorber is due to the air-gap mode resonance, the first-order grating diffraction, and the second-order grating diffraction (three peaks in the upper image of Fig. 9(e)). When the carrier density is $N=1.6\times10^{16}$ cm^{-3} (with the resistivity of 0.54 $\Omega.cm$), such a heavily doped silicon-based grating structure can have metallic behavior, which means that the loss of the

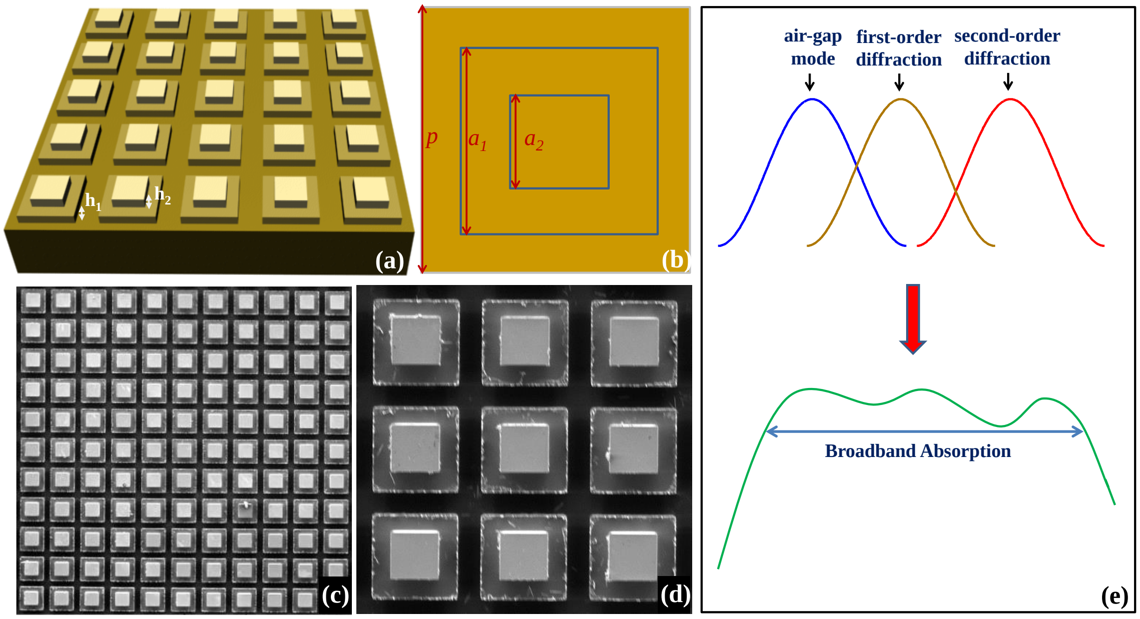

Fig. 9 Configuration and principle of the broadband THz absorber. (a) and (b) Schematic diagram of the sample. (c) and (d) SEM of the fabricated sample. (e)The fundament principle of such ultra-broadband THz absorber.

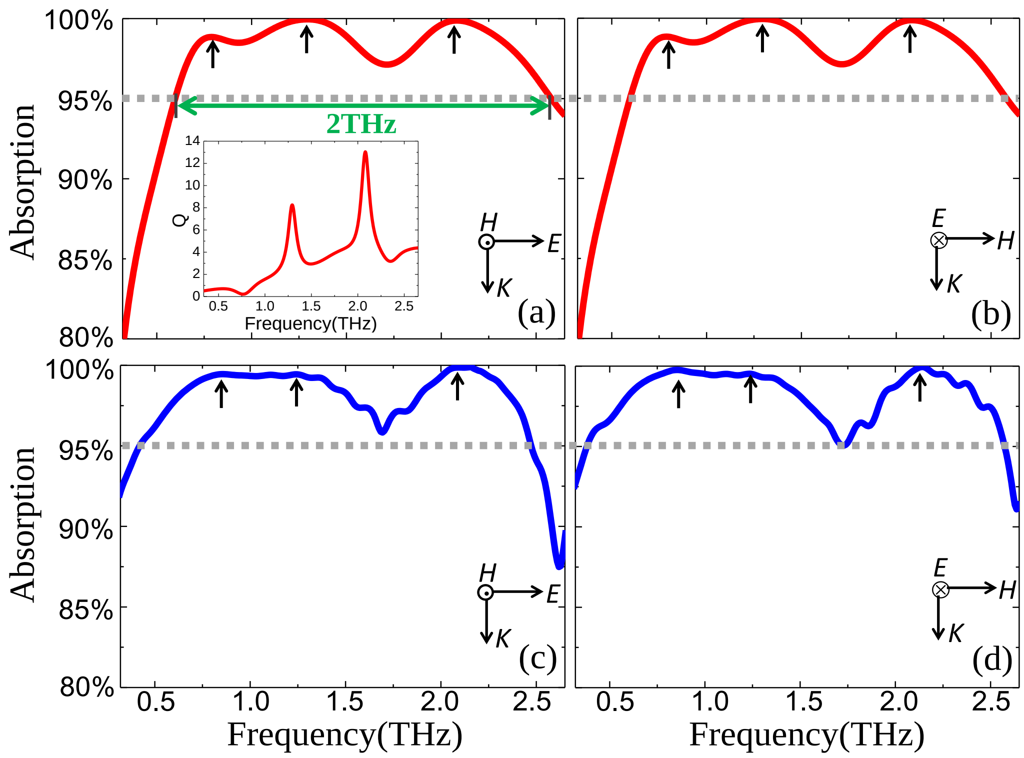

Fig. 10 Calculated ((a), (b)) and measured ((c), (d)) absorption spectra of the THz absorber. (a) and (c) for TE incident THz wave, (b) and (d) for TM incident THz wave. The inset in (a) is the corresponding quality factor of the THz absorber.

doped-silicon is very high and the corresponding quality factor is very low (see the inset in Fig. 10(a)). These three peaks can be broadened in such relatively high-loss material. So, all of these three broadened peaks can be combined into each other, resulting in an ultra-broadband THz absorber. The structure parameters are p=100 μm, a_1=80 μm, and a_2=45 μm. $h_{grating}$=40 μm (h_1=h_2=40 μm, thickness of the up and down gratings) and $h_{substrate}$=420 μm, respectively.

For TE and TM THz wave, the incident THz waves can be efficiently absorbed over 95% (see the simulated results in Figs. 10(a) and 10(b)) from 0.59 to 2.58 *THz*, with the absorption bandwidth nearly about 2 *THz*. The experimental measured results are presented in Figs. 10(c) and 10(d), where the absorption efficiency is over 95% with bandwidth of more than 2 *THz* for both TE and TM incident waves. It can be found that the measured and the calculated results show good agreement, except for a slight discrepancy in the resonant frequency, due to the difference between the calculated models and the fabricated structure. In addition, both of them have three peaks at f=0.789 *THz*, f=1.294 *THz*, and f=2.083 *THz*, respectively in the absorption spectra. Therefore, such an ultra-broadband THz absorber is attributed to these three peaks, which are labeled by three arrows in Fig. 10.

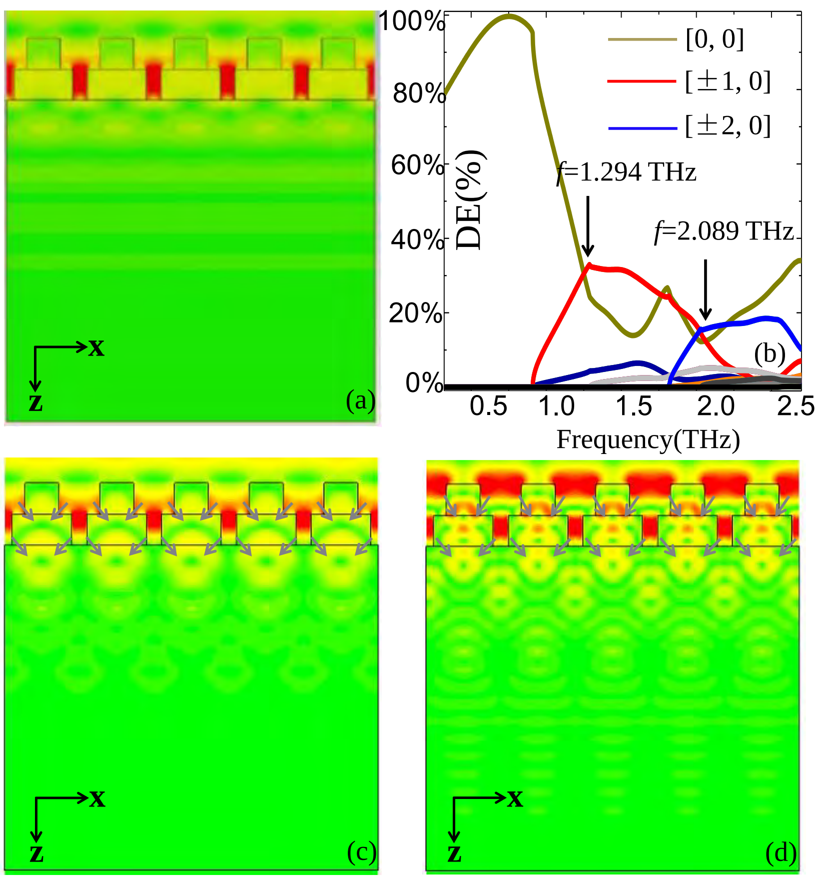

Fig. 11 (a)The field distributions of the double layered grating array at f=0.789 *THz*. (b) The diffraction efficiency (DE) of different diffraction orders. (c), (d) The field distributions of the double layered grating array at 1.294 *THz* and 2.083 *THz*, respectively.

Now, we study the mechanism of these three resonance peaks. Figure. 11(a) shows the electric field distribution of the double layered grating array at *f*=0.789 *THz*. In this case, the incident THz wave is mainly located in the air gap between the bottom grating array, and there is a little incident THz wave transmitted into the substrate. This is verified that the left peak at *f*=0.789 *THz* is caused by the air gap in the bottom grating array, and it can be defined as local air gap resonance mode. In the high-frequency regime, the grating diffractions can be utilized to explain these two peaks at *f*=1.294 *THz*, and *f*=2.083 *THz*, respectively. We also calculate the grating diffraction of such double-layered grating structure, as shown in Fig. 11(b). Obviously, these two peaks at *f*=1.294 *THz*, and *f*=2.083 *THz* are mainly caused by the [±1, 0]-order and [±2, 0]-order grating diffractions, respectively. The corresponding field distributions of these two peaks are shown in Figs. 11(c) and 11(d), and we can find that part of power is transmitted into the substrate through the air gap (see the arrows in Figs. 11(c) and 4(d)). Therefore, we can conclude that such an ultra-broadband THz absorber is caused by combining the air gap resonance mode, the [±1, 0]-order and [±2, 0]-order grating diffractions.

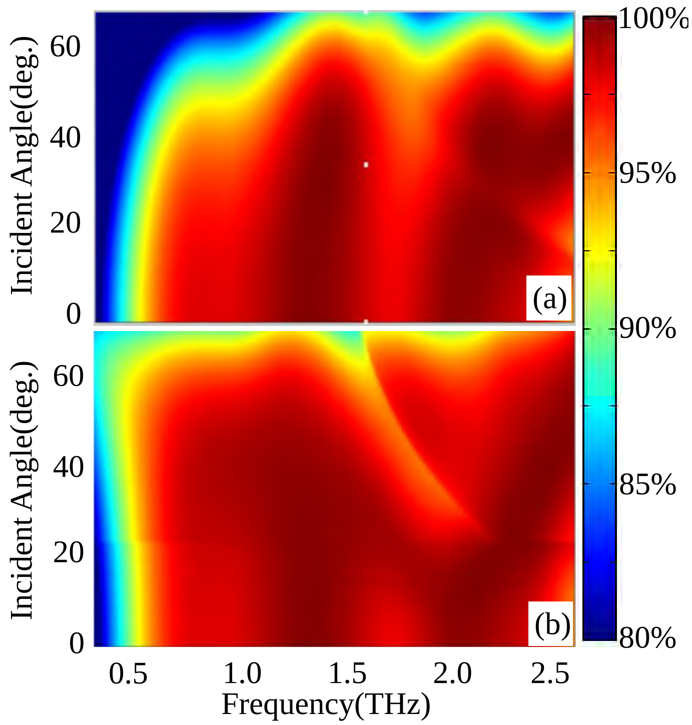

Fig. 12 The absorption spectra with different incidence angles for (a)TE THz wave, and (b)TM THz wave.

For non-normal incident wave, our designed ultra-broadband THz absorber can also produce effect adequately, as shown in Figs. 12(a) and 12(b). For TE THz wave, the absorption efficiency is also above 95% with bandwidth 2 *THz*, when the oblique angle as large as 45^{o}. For TM THz wave, the absorption efficiency can still maintain above 95% with bandwidth 2 *THz*, when the oblique angle is larger than 55^{o}. Therefore, our ultra-broadband THz absorber can be operated in a larger oblique incident angle.

5. Conclusions

In summary, we have reviewed three kinds of grating structure to realize broadband polarization-independent THz absorber. The first is a square-shaped grating which can cause the anti-reflection effects (destructive interference) in the low frequency regime and the [±1, 0]-order diffraction in the high frequency regime. By optimizing the structure parameters, both of the anti-reflection effects and the [±1, 0]-order diffraction can be jointed into each other, leading to a broadband THz absorber with bandwidth of 1 *THz*. The second is a dumbbell-shaped broadband THz absorber (the absorption bandwidth is 1.5 *THz*), which is caused by the anti-reflection effects, the [±1, 0]-order and the [0, ±1]-order diffractions. The last is double-layered square grating-shaped ultra-broadband THz absorber (the absorption bandwidth is 2.0 *THz*), which is mainly attributed to the air gap resonance mode, the [±1, 0]-order and [±2, 0]-order grating diffractions. Our proposed broadband THz absorber may be applied into THz imaging system, anti-radar cloaking, filter, sensor and so on.

References

[1] A. Giugni, B. Torre, A. Toma, et.al. "Hot-electron nanoscopy using adiabatic compression of surface plasmons". *Nat. Nanotechnol.*, 8, 845-852 (2013).

[2] P. James Schuck. "Nanoimaging: Hot electrons go through the barrier". *Nat. Nanotechnol.*, 8, 799-800 (2013).

[3] V. E. Ferry, M. A. Verschuuren, H. B. Li, et al. "Light trapping in ultrathin plasmonic solar cells". *Opt. Express* 18, A237-A245 (2010)

[4] F. Alves, D. Grbovic, B. Kearney, et al. "Microelectromechanical systems bimaterial terahertz sensor with integrated metamaterial absorber". *Opt. Lett.*37, 1886-1888 (2012)

[5] M. W. Knight, H. Sobhani, P. Nordlander, et al. "Photodetection with Active Optical Antennas". *Science*. 332, 702-704 (2011).

[6] A. Sobhani, M. W. Knight, Y. Wang, et al. "Narrowband photodetection in the near-infrared with a plasmon-induced hot electron device". *Nat. Commun*. 4, 1643-1647 (2013).

[7] L. O'Faolain, D. M. Beggs, T. P. White, et al. "Compact optical switches and modulators based on dispersion engineered photonic crystals". *IEEE Photon. J*. 2, 404–414 (2010).

[8]H. Chalabi, D. Schoen, and M. L. Brongersma. "Hot-Electron Photodetection with a Plasmonic Nanostripe Antenna". *Nano. Lett*. 14, 1374-1380 (2014).

[9] N. I. Landy, S. Sajuyigbe, J. J. Mock, et al. "Perfect metamaterial absorber". *Phys. Rev. Lett.* 100, 207402 (2008).

[10] H. Tao, N. I. Landy, C. M. Bingham, et al. "A metamaterial absorber for the terahertz regime: Design, fabrication and characterization". *Opt. Express*. 16, 7181-7188 (2008).

[11] C. M. Bingham, H. Tao, X. Liu, et al. "Planar wallpaper group metamaterials for novel terahertz applications". *Opt. Express*. 16, 18565-18575 (2008).

[12] Y. Avitzour, Y. A. Urzhumov, and G. Shvets. “Wide-angle infrared absorber based on a negative-index plasmonic metamaterial”. *Phys. Rev. B.* 79, 045131 (2008).

[13] N. I. Landy, C. M. Bingham, T. Tyler, et al. “Design, theory, and measurement of a polarization-insensitive absorber for terahertz imaging”. *Phys. Rev. B.* 79, 125104 (2008).

[14] X. Liu, T. Starr, A. F. Starr, et al. “Infrared spatial and frequency selective metamaterial with near-Unity absorbance”. *Phys. Rev. Lett.* 104, 207403 (2010).

[15] K. Aydin, V. E. Ferry, R. M. Briggs, et al. “Broadband polarization-independent resonant light absorption using ultrathin plasmonic super absorbers”. *Nat. Commun*. 2, 517-523 (2011).

[16] Y. Q. Xu, P. H. Zhu, H. B. Zhang, et al. “A wide-angle planar metamaterial absorber based on split ring resonator coupling”. *J. Appl. Phys.* 110, 044102 (2011).

[17] B. Wang, T. Koschny, and C. M. Soukoulis. “Wide-angle and polarization-independent chiral metamaterial absorber”. *Phys. Rev. B*. 80, 033108 (2009).

[18] Y. Q. Ye, Y. Jin, and S. L. He. “Omnidirectional, polarization-insensitive and broadband thin absorber in terahertz regimem”. *J. Opt. Soc. Am. B* 27, 498-504 (2010).

[19] J. Hao, J. Wang, X. Liu, et al. “High performance optical absorber based on a plasmonic metamaterial”. *Appl. Phys. Lett.* 96, 251104 (2011).

[20] N. Liu, M. Mesch, T. Weiss, et al. “Infrared Perfect Absorber and Its Application As Plasmonic Sensor”. *Nano. Lett.* 10, 2342 (2010).

[21] H.-T. Chen, J. F. Zhou, J. F. O’Hara, et al. “Antireflection coating using metamaterials and identification of its mechanism”. *Phys. Rev. lett.* **105**, 073901 (2010).

[22] Y. Ma, Q. Chen, J. Gran, et al. “A terahertz polarization insensitive dual band metamaterial absorber”. *Opt. Lett.* 36, 945-947 (2011).

[23] H.-T. Chen. “Interference theory of metamaterial perfect absorbers”. *Opt. Express.* 20, 7165-7172 (2012).

[24] Z. H. Jiang, S. Yun, F. Toor, et al. “Conformal Dual-Band Near-Perfectly Absorbing Mid-Infrared Metamaterial Coating”. *ACS Nano*. 5, 4641-4647 (2011).

[25] J. Wang, Y. T. Chen, J. M. Hao, et al. “Shape-dependent absorption characteristics of three-layered metamaterial absorbers at near-infrared”. *J. Appl. Phys.* 109, 074510 (2011).

[26] K. B. Alici, A. B. Turhan, C. M. Soukoulis, et al. “Optically thin composite resonant absorber at the near-infrared band: a polarization independent and spectrally broadband configuration”. *Opt. Express* 19, 14260-14267 (2011).

[27] Y. Ma, Q. Chen, J. Grant, et al. “A terahertz polarization insensitive dual band metamaterial absorber”. *Opt. Lett.* 36, 945-947 (2011).

[28] B. Zhang, Y. Zhao, Q. Hao, et al. “Polarization-independent dual-band infrared perfect absorber based on a metal-dielectric-metal elliptical nanodisk array”. *Opt. Express.* 19, 15221-15228 (2011).

[29] X. Shen. T. Cui, J. Zhao, et al. “Polarization-independent wide-angle triple-band metamaterial absorber”. *Opt. Express.* 19, 9401-9407 (2011).

[30] X. Shen, Y. Yang, Y. Zang, et al. “Triple-band terahertz metamaterial absorber: Design, experiment, and physical interpretation”. *Appl. Phys. Lett*. 101, 154102 (2012).

[31] L. Huang, D. R. Chowdhury, S. Ramani, et al. “Experimental demonstration of terahertz metamaterial absorbers with a broad and flat high absorption band”. *Opt. Lett*. 37, 154-156 (2012).

[32] C. Wu, and G. Shvets. “Design of metamaterial surfaces with broadband absorbance”. *Opt. Lett*. 37, 308-310 (2012).

[33] J. Hendrickson, J. Gao, B. Zhang, et al. “Wideband perfect light absorber at midwave infrared using multiplexed metal structures”. *Opt. Lett*. 37, 371-373 (2012).

[34] Q. Feng, M. Pu, C. Hu, et al. “Engineering the dispersion of metamaterial surface for broadband infrared absorption”. *Opt. Lett*. 37, 2133-2135 (2012).

[35] Y. X. Cui, K. H. Fung, J. Xu, et al. “Ultrabroadband light absorption by a sawtooth anisotropic metamaterial slab”. *Nano. Lett.* 12, 1443-1447 (2012).

[36] F. Ding, Y. X. Cui, X. Ge, et al. “Ultra-broadband microwave metamaterial absorber”. *Appl. Phys. Lett*. 100, 103506 (2012).

[37] D. Ye, Z. Wang, K. Xu, et al. “Ultrawideband dispersion control of a metamaterial surface for perfectly-matched-layer-Like absorption”. *Phys. Rev. lett.* 111, 187402 (2013).

[38] W. Li, T. Wu, W. Wang, et al. “Integrating non-planar metamaterials with magnetic absorbing materials to yield ultra-broadband microwave hybrid absorbers”. *Appl. Phys. Lett.* 104, 022903 (2014).

[39] R. Kakimi, M. Fujita, M. Nagai, et al. “Capture of a terahertz wave in a photonic crystal slab”. *Nat. Photon.* 8, 657-663 (2014)

[40] M. Pu, M. Wang, C. Hu, et al. “Engineering heavily doped silicon for broadband absorber in the terahertz regime”. *Opt. Express* 20, 25513-25519 (2012).

[41] S. Yin, J. Zhu, W. Xu, et al. “High-performance terahertz wave absorbers made of silicon-based metamaterials”. *Appl. Phys. Lett*. 107, 073903 (2015).

[42] C. Shi, X. F. Zang, Y. Q. Wang, et al. “A polarization-independent broadband terahertz absorber”. *Appl. Phys. Lett.* 105, 031104 (2014).

[43] X. Zang, C. Shi, L. Chen, et al. “Ultra-broadband terahertz absorbsorption by exciting the orthogonal diffraction in dumbbell-shaped gratings”. *Sci. Rep*. 5, 8901 (2015)

[44] Y. Peng, X. Zang, Y. Zhu, et al. “Ultra-broadband terahertz perfect absorber by exciting multi-order diffractions in a double-layered grating structure”. *Opt. Express.* 23, 2032-2039 (2015).

[45] C. C. Katsidis and D. I. Siapkas. “General transfer-matrix method for optical multilayer systems with coherent, partially coherent, and incoherent interference”. *Appl. Opt.* 41, 3978-3987 (2002).

[46] D. E. Aspnes. “Local field effects and effective medium theory: A microscopic perspective”. *Am. J. Phys.* 50, 704 (1982).

[47] R. Bräuer and O. Bryngdahl. “Design of antireflection gratings with approximate and rigorous methods”. *Appl. Opt*. 33, 7875-7882 (1994).